Generalized Image Navigation and Registration Method Based on Kalman Filter

Ahmed A. Kamel, Handol Kim, Dochul Yang, Chulmin Park and Jin Woo

Nomenclature

R_{so}:	ideal geosynchronous radius = 42164000 m
λ_{so}:	ideal satellite longitude
ω_e:	sidereal earth rotation rate = 7.2921159E-05 rad/s
R, L,λ:	radius, geocentric latitude, longitude
R_{eo}:	equatorial radius = 6378136.6 m
f:	earth flattening = 1/298.25642
h:	landmark altitude
ϕ, θ, ψ:	roll, pitch, yaw
ECLF:	earth centered local frame
GEOS:	fixed grid frame
LOS:	line of sight
LRF:	LOS reference frame
IIRF:	imager internal reference frame
ACF:	attitude control frame
ORF:	orbit reference frame

A.A. Kamel (✉)
Kamel Engineering Services, Los Angeles, CA, USA
e-mail: ahmed@kamelengineering.com

H. Kim · D. Yang
Korea Aerospace Research Institute, Daejeon, Republic of Korea
e-mail: hkim@kari.re.kr

D. Yang
e-mail: dcyang@kari.re.kr

C. Park
Korea Aerospace Industries, Sacheon, Republic of Korea
e-mail: cmpark@koreaaero.com

J. Woo
Korea Meteorological Administration, Seoul, Republic of Korea
e-mail: superjwoo@korea.kr

B. Dołęga et al. (eds.), *Advances in Aerospace Guidance, Navigation and Control*, https://doi.org/10.1007/978-3-319-65283-2_33

I_{ixi}, 0_{ixj}: ixi identity matrix, ixj null matrix
S, C: Sin, Cos
EW, NS: East-West, North-South

Subscripts

0, s, e: initial, satellite, earth
T: landmark point on earth
ma: misalignment
m: number of imager internal misalignment
att: spacecraft attitude from telemetry
corr: thermoelastic/attitude correction angles

1 Introduction

The term image navigation and registration and the INR acronym were coined by Kamel [1] and patented in US Patents # 4,688,091, 4,688,092, and 4,746,976 to represent a system that determines image pixel location and register it to fixed grid frame (called FGF in GOES and GEOS in COMS and in this paper). This INR invention became the foundation for subsequent GOES and similar systems worldwide [2–5]. The INR system requirements tightened as spacecraft and ground hardware improved [6–9].

The image navigation part of INR relates to LOS absolute pointing. Section 2 defines the INR and KF state vectors needed for this process. Section 3 describes new INR method (patent application being filed in ROK) based on landmark measurements to determine orbit, attitude correction, and imager misalignments with maneuvers delta V provided by FDS. Also, orbit refinement can be made if FDS provides orbit with coarse accuracy instead of delta V. Section 4 shows the simulation results of this basic system. Section 5 shows how the new method can be adapted to be used for other INR systems implemented nowadays.

The image registration part of INR relates to LOS stability. The objective of image registration is to provide the users with images with pixels that have the same fixed earth location regardless of time. Section 6 provides an algorithm for transferring pixels from LOS frame to GEOS frame needed for pixel data resampling in GEOS frame.

2 INR and KF SV Definitions

The INR and KF SV definitions and the associated time series are given in the next three subsections.

2.1 INR SV Definition

The INR SV is required for transformation from LRF to GEOS for Sect. 3.1.2. This is given by:

$$SV_{INR} = [SV_{ma}^{T}\ SV_{corr}^{T}\ SV_{att}^{T}\ SV_{orb}^{T}]^{T} \tag{1}$$

SV_{ma} is based on IIRF misalignment relative to LRF.
SV_{corr}, SV_{att}, and SV_{orb} are based on:
$(\phi_{corr}\ \theta_{corr}\ \psi_{corr})$ = ACF attitude relative to IIRF.
$(\phi_{att}, \theta_{att}, \psi_{att})$ = ORF attitude relative to ACF.
$(\phi_{orb}, \theta_{orb}, \psi_{orb})$ = GEOS attitude relative to ORF.

For single mirror imagers, such as GOES I-P, COMS, MTSAT2, SV_{ma} is given by:

$$SV_{ma} = [\phi_{ma}\ \theta_{ma}]^{T} \tag{2.1}$$

$$= SV_{ma,model} + x_{ma} \tag{2.2}$$

$$SV_{ma,model} = [\phi_{ma,model}\ \theta_{ma,model}]^{T}$$

$$SV_{corr} = [\phi_{corr}\ \theta_{corr}\ \psi_{corr}]^{T} \tag{3.1}$$

$$= SV_{corr,model} + x_{corr} \tag{3.2}$$

$$SV_{corr,model} = [\phi_{corr,model}\ \theta_{corr,model}\ \psi_{corr,model}]^{T}$$

The thermoelastic misalignment and correction models are computed in Sect. 3.4 and (x_{ma}, x_{corr}) are defined in Sect. 2.2 and determined by KF.

$$SV_{att} = [\phi_{att}\ \theta_{att}\ \psi_{att}]^{T} \text{ from telemetry} \tag{4}$$

$$SV_{orb} = [R_s \quad \Delta\lambda_s \quad L_s\ ]^{T} \tag{5.1}$$

$$R_s = R_{so}\left(1 + \frac{\Delta R_s}{R_{so}}\right),\ \Delta\lambda_s = \lambda_s - \lambda_{so} \tag{5.2}$$

For 3,1,2 type rotation, SV_{ORF} is given by:

$$SV_{ORF} = [\phi_{orb}\ \theta_{orb}\ \psi_{orb}]^{T} \tag{6.1}$$

For Spacecraft x axis parallel to earth equator (e.g., COMS):

$$SV_{ORF} = [L_s\ \Delta\lambda_s\ 0]^{T} \tag{6.2}$$

For Spacecraft x axis parallel to orbit plane (e.g., GOES I-M):

$$SV_{ORF} = [L_s \; \Delta\lambda_s \; \dot{L}_s/\omega_e]^T \tag{6.3}$$

$\left(\frac{\Delta R_s}{R_{so}}, \Delta\lambda_s, L_s \; \dot{L}_s/\omega_e\right)$ are Kamel parameters [10, 11] originally used for GOES I-M.

If FDS provides maneuver delta V:

$$\frac{\Delta R_s}{R_{so}} = \frac{\delta R_s}{R_{so}}, \Delta\lambda_s = \delta\lambda_s, L_s = \delta L_s, L_s = \delta L_s \tag{7.1}$$
$$\left(\frac{\delta R_s}{Rso}, \delta\lambda_s, \delta L_s, \delta \dot{L}_s\right) = \text{ideal ordeal refinement by KF.}$$

If FDS provides orbit instead of maneuver delta V:

$$\begin{aligned} &R_s = Rso\left[\frac{R_{FDS}}{Rso} + \frac{\delta R_s}{Rso}\right] \Delta\lambda_s = \Delta\lambda_{FDS} + \delta\lambda_s, \\ &L_s = L_{FDS} + \delta L_s, \dot{L}_s = \dot{L}_{FDS} + \delta \dot{L}_s \\ &\left(\frac{\delta R_s}{Rso}, \delta\lambda_s, \delta L_s, \delta \dot{L}_s\right) = \text{FDS ordeal refinement by KF.} \end{aligned} \tag{7.2}$$

2.2 *KF SV Definition*

$SV_{KF} = x$ is needed to determine SV_{INR} of Sect. 2.1. This is defined as follows:

$$X = [X_{corr}^T \quad \dot{X}_{corr}^T \quad X_{orb}^T \quad \dot{X}_{orb}^T \quad X_{ma}^T \quad \dot{X}_{ma}^T]^T \tag{8.1}$$
$$X_{corr} = [\delta\,\phi_{corr} \quad \delta\,\theta_{corr} \; \delta\,\psi_{corr}]^T \tag{8.2}$$
$$\dot{X}_{corr} = \left[b_{\phi_{corr}} \quad b_{\theta_{corr}} \quad b_{\psi_{corr}}\right]^T = \text{constant} \tag{8.3}$$
$$X_{orb} = \left[\frac{\delta R_s}{R_{so}} \quad \delta\lambda_s \quad \delta L_s\right]^T \tag{8.4}$$
$$\dot{X}_{orb} = \left[\frac{\delta \dot{R}_s}{R_{so}} \quad \delta\dot{\lambda}_s \quad \lambda\dot{L}_s\right]^T \tag{8.5}$$
$$X_{ma} = [\delta\,\phi_{ma} \quad \delta\,\theta_{ma}]^T \tag{8.6}$$
$$\dot{X}_{ma} = [b_{\phi_{ma}} \quad b_{\theta_{ma}}]^T = \text{constant} \tag{8.7}$$

At KF start, $x = 0_{12+2m}$.

2.3 SV Time Series

SV_{INR} time series are generated at points spaced by Δt_i for image registration of Sect. 6. This requires interpolation between SV_{KF} time series points determined by landmarks (or star measurements) time series points based on attitude telemetry (e.g., at one second interval) and FDS orbit, $SV_{ma,model}$, and $SV_{corr,model}$ time series (e.g., at one minute interval). The SV_{KF} time series between measurements can be obtained as follows:

$$X(t_i) = A(\Delta t_i)X(t_0), \quad \Delta t_i = t_i - t_i - t_0, t_0 \le t_i \le t_1 \tag{9.1}$$

$$A(\Delta t_i) = \begin{bmatrix} A_{corr}(\Delta t_i) & 0_{6\times 6} & 0_{6\times 2m} \\ 0_{6\times 6} & A_{orb}(\Delta t_i) & 0_{6\times 2m} \\ 0_{2m\times 6} & 0_{2m\times 6} & A_{ma}(\Delta t_i) \end{bmatrix} \tag{9.2}$$

$$A_{corr}(\Delta t_i) = \begin{bmatrix} I_{3\times 3} & I_{3\times 3}\Delta t_i \\ 0_{3\times 3} & I_{3\times 3} \end{bmatrix} \tag{9.3}$$

$A_{orb}(\Delta t_i)$ obtained from the well-known Euler-Hill equations [12]

$$A_{orb}(\Delta t_i) = \begin{bmatrix} A_{11} & A_{12} \\ A_{21} & A_{22} \end{bmatrix} \tag{9.4}$$

$$A_{11} = \begin{bmatrix} (4-3\,C) & 0 & 0 \\ 6(S-\gamma) & 1 & 0 \\ 0 & 0 & C \end{bmatrix} \tag{9.5}$$

$$A_{12} = \begin{bmatrix} \omega_e^{-1}S & 2\omega_e^{-1}(1-C) & 0 \\ -2\omega_e^{-1}(1-C) & \omega_e^{-1}(4S-3\,\gamma) & 0 \\ 0 & 0 & \omega_e^{-1}S \end{bmatrix} \tag{9.6}$$

$$A_{21} = \begin{bmatrix} 3\omega_e S & 0 & 0 \\ 6\omega_e^{-1}(C-1) & 0 & 0 \\ 0 & 0 & -\omega_e S \end{bmatrix} \tag{9.7}$$

$$A_{22} = \begin{bmatrix} C & 2\,S & 0 \\ -2\,S & (4C-3) & 0 \\ 0 & 0 & C \end{bmatrix} \tag{9.8}$$

$$C = \mathrm{Cos}\ \gamma,\quad S = \mathrm{Sin}\ \gamma,\quad \gamma = \omega_e \Delta t_i,\quad \omega_e^{-1} = \frac{1}{\omega_e}.$$

For small Δt_i, $C = 1$ and $S = \gamma = \omega_e \Delta t_i$,

$$A_{orb}(\Delta t_i) = \begin{bmatrix} I_{3\times3} & I_{3\times3}\Delta t_i \\ 0_{3\times3} & I_{3\times3} \end{bmatrix} \tag{9.9}$$

Note that Euler-Hill equations used to model orbit and Sect. 3.4 used to model thermoelastic angles leads to significant reduction of the number of landmarks processed by KF compared to using simple linear models that are only valid for short time.

$$A_{ma}(\Delta t_i) = \begin{bmatrix} I_{m\times m} & I_{m\times m}\Delta t_i \\ 0_{m\times m} & I_{m\times m} \end{bmatrix} \tag{9.10}$$

m = number of imager internal misalignments.

For single mirror imager used for GOES I-P, COMS, MTSAT2 and in this paper, m = 2. For two mirror imagers, the number of misalignments depend on the thermoelastic effect on pointing. The leading term was called Orthogonality (O_{ma}) by Kamel because it represents deviation of the scanning axes from being perpendicular. Note that if only O_{ma} has significant effect on pointing [11], the number of misalignments m = 1.

3 Image Navigation Using KF

Figure 1 shows KF flow for the basic INR method. KF uses one landmark at a time to determine best (a-posteriori) state vector and covariance matrix estimate (x_1^+, P_1^+). KF is then re-initialized to make propagation always between t_0 and t_1 and estimation at t_1.

The 3-step process is as follows:

1. a-priori state vector and covariance matrix (x_1^-, P_1^-) obtained from (x_0^+, P_0^+) using the transition matrix $A(\Delta t)$, $\Delta t = t_1 - t_0$ and error matrix $Q(\Delta t)$ obtained from system model. This first step is called SV and covariance matrix P propagation

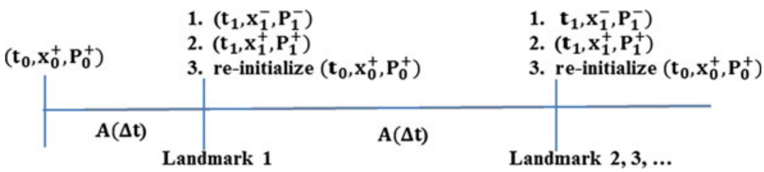

Fig. 1 Kalman filter for the basic INR method

between two successive landmarks.

$$x_1^- = A(\Delta t)x_0^+ \tag{10.1}$$

$$P_1^- = A(\Delta t)P_0^+ A(\Delta t)^T + Q(\Delta t) \tag{10.2}$$

2. (x_1^+, P_1^+) obtained from (x_1^-, P_1^-) and measurement model (Z, H,R). This second step is called SV and covariance matrix P estimation at t_1. Kalman assumed the relation- ship between $x_1^+$and x_1^- is given by a form like least squares and determined associated Kalman gain matrix K and covariance matrix P:

$$x_1^+ = x_1^- - K\Delta Z,\ \Delta Z = Z - \bar{Z} \tag{11.1}$$

$$K = P_1^- H^T (HP_1^- H^T + R)^{-1} \tag{11.2}$$

$$P_1^+ = (I - KH)P_1^-(I - KH)^T + KRK^T \tag{11.3}$$

The residual ΔZ is computed as follows:

- Compute SV_{INR} from x_1^- using Sects. 2.1 and 2.2.
- Compute landmark residuals using Sect. 3.1.
- If landmark is rejected because residual is outside predetermined limit:
  - Re-initialize KF: $(t_0, x_0^+, P_0^+) = (t_1, x_1^+, P_1^+) = (t_1, x_1^-, P_1^-)$.
  - Skip estimation and go to next landmark.

If landmark is accepted, compute x_1^+ using Eq. (11.1).
Note that $(\Delta x_{corr}^+, \Delta x_{orb}^+, \Delta x_{ma}^+) = (x_{corr}^+, x_{orb}^+, x_{ma}^+) - (x_{corr}^-, x_{orb}^-, x_{ma}^-)$ obtained from Eq. (11.1) can cause jumps in level 1B images at t_1. This can be avoided by replacing $(\dot{x}_{corr}^+, \dot{x}_{orb}^+, \dot{x}_{ma}^+)$ [also obtained from Eq. (11.1) and given by Eqs. (8.3), (8.5) and (8.7)] with $(\dot{x}_{corr}^+, \dot{x}_{orb}^+, \dot{x}_{ma}^+) + (\Delta x_{corr}^+, \Delta x_{orb}^+, \Delta x_{ma}^+)/\,\delta t$, where, δt = delta time to next landmark or next KF point. After this slope adjustment, set $(x_{corr}^+, x_{orb}^+, x_{ma}^+) = (x_{corr}^-, x_{ma}^-, x_{ma}^-)$ at t_1.

3. The third step is to re-initialize KF by setting $(t_0, x_0^+, P_0^+) = (t_1, x_1^+, P_1^+)$ to start the next cycle from t_0 to t_1 and compute SV_{INR} from x_1^+ using Sect. 2. This is needed for Sect. 6.

3.1 KF Landmark Residual Computation

The landmark residuals $\Delta Z = Z - \bar{Z}$ are computed from the next two subsections.

3.1.1 Actual Landmark Measurement $\bar{Z}$

In view of Fig. 2, we get:

$$\vec{R}_{To} = \vec{T} - \vec{R}_{So} \tag{12.1}$$

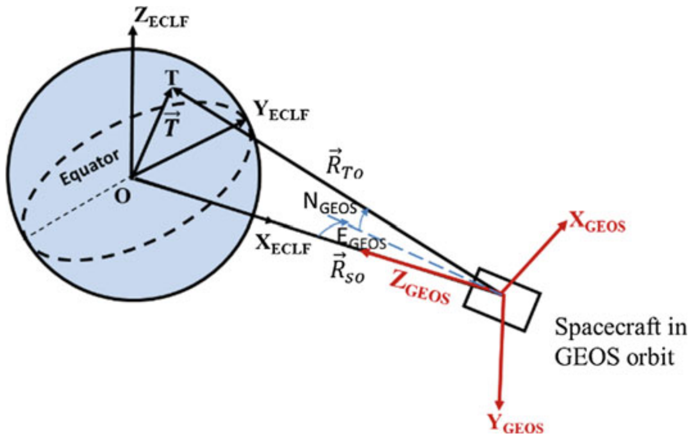

Fig. 2 ECLF to GEOS geometry

Using vector components in GEOS coordinates, we get:

$$\vec{R}_{To} = (R_e + h)\begin{bmatrix} C_{L_T} S_{\Delta\lambda_T} \\ -S_{L_T} \\ -C_{L_T} C_{\Delta\lambda_T} \end{bmatrix} - R_{so}\begin{bmatrix} 0 \\ 0 \\ -1 \end{bmatrix} = R_{To}\begin{bmatrix} C_{\bar{N}_{GEOS}} S_{\bar{E}_{GEOS}} \\ -S_{\bar{N}_{GEOS}} \\ C_{\bar{N}_{GEOS}} C_{\bar{E}_{GEOS}} \end{bmatrix} \quad (12.2)$$

$$R_e = R_{eo}(1 + aS_{L_T}^2)^{-\frac{1}{2}} \cong R_{eo}(1 - f\, S_{L_T}^2) \quad (12.3)$$

$$\Delta\lambda_T = \lambda_T - \lambda_{so},\ a = (1 - f)^{-2} - 1 \cong 2f \quad (12.4)$$

This leads to:

$$R_{To} = \sqrt{R_{so}^2 + (R_e + h)^2 - 2R_{so}(R_e + h)C_{L_T} C_{\Delta\lambda_T}} \quad (13.1)$$

$$\bar{E}_{GEOS} = \text{Arc tan}\left[\frac{(R_e + h)C_{L_T} S_{\Delta\lambda_T}}{R_{so} - (R_e + h)C_{L_T} C_{\Delta\lambda_T}}\right] \quad (13.2)$$

$$\bar{N}_{GEOS} = \text{Arc sin}\left[\frac{(R_e + h)S_{L_T}}{R_{To}}\right] \quad (13.3)$$

$$\bar{Z} = \begin{bmatrix} \bar{E}_{GEOS} \\ \bar{N}_{GEOS} \end{bmatrix} \quad (13.4)$$

3.1.2 Estimated Landmark Measurement Z

Transformation of landmark (E_{LRF}, N_{LRF}) coordinates to (E_{GEOS}, N_{GEOS}) coordinates is obtained in the next 4 subsections.

3.1.2.1 $\widehat{U}_{IIRF}$ and $\widehat{R}_{IIRF}$ Computation

For single mirror instruments:

$$E_{IIRF} = E_{LRF} - (\phi_{ma} S_{N_{LRF}} + \theta_{ma} C_{N_{LRF}}) \tag{14.1}$$

$$N_{IIRF} = N_{LRF} - (\phi_{ma} C_{N_{LRF}} - \theta_{ma} S_{N_{LRF}})/C_{E_{LRF}} \tag{14.2}$$

(E_{LRF}, N_{LRF}) = determined landmark (EW, NS) angles.

To get (E_{LRF}, N_{LRF}) from (E_{IIRF}, N_{IIRF}) for inverse transformation, two iterations of Eqs. (14.1) and (14.2) may be needed.

The unit vector $\widehat{U}_{IIRF}$ components in IIRF coordinates is obtained by a rotation N_{IIRF} about X-axis followed by a rotation E_{IIRF} about new Y-axis. This leads to:

$$\widehat{U}_{IIRF} = \begin{bmatrix} S_{E_{IIRF}} \\ -C_{E_{IIRF}} S_{N_{IIRF}} \\ C_{E_{IIRF}} C_{N_{IIRF}} \end{bmatrix} \tag{14.3}$$

The unit vector $\widehat{R}_{IIRF}$ components in GEOS is given by:

$$\widehat{R}_{IIRF} = C_{IIRF}^{GEOS} \widehat{U}_{IIRF} = [\widehat{R}_{GEOS,X} \quad \widehat{R}_{GEOS,Y} \quad \widehat{R}_{GEOS,Z}]^T \tag{14.4}$$

Note that for inverse transformation, use:

$$\widehat{U}_{IIRF} = C_{GEOS}^{IIRF} \widehat{R}_{IIRF}, \; C_{GEOS}^{IIRF} = [C_{IIRF}^{GEOS}]^T \tag{14.5}$$

3.1.2.2 IIRF to GEOS Transformation Matrix Computation

Transformation from IIRF to GEOS is 3,1,2, type rotation and can be obtained from Appendix E, Table E-1, Ref. [13] by replacing (ϕ, θ, ψ) with (ψ_C, ϕ_C, θ_C):

$$\begin{aligned} C_{IIRF}^{GEOS} &= \begin{bmatrix} C_\theta C_\psi - S_\theta S_\phi S_\psi & C_\theta C_\psi + S_\theta S_\phi S_\psi & -S_\theta C_\phi \\ -S_\psi C_\phi & C_\psi C_\phi & S_\phi \\ S_\theta C_\psi + C_\theta S_\phi S_\psi & S_\theta S_\psi - C_\theta S_\phi C_\psi & C_\phi C_\theta \end{bmatrix}_C \\ &\cong \begin{bmatrix} 1 & \psi_C & -\theta_C \\ -\psi_C & 1 & \phi_C \\ \theta_C & -\phi_C & 1 \end{bmatrix} \end{aligned} \tag{15.1}$$

In view of Eqs. (3.1), (4), and (6.1) to (6.3) we get:

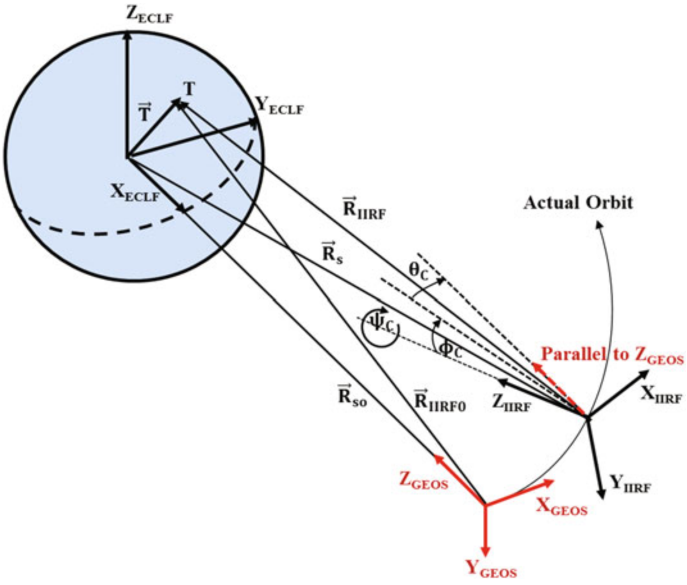

Fig. 3 Image navigation geometry

$$SV_C = \begin{bmatrix} \phi_c \\ \theta_C \\ \psi_C \end{bmatrix} = SV_{ACF} + SV_{corr} \tag{15.2}$$

$$SV_{ACF} = \begin{bmatrix} \phi \\ \theta \\ \psi \end{bmatrix} = SV_{ORF} + SV_{att} \tag{15.3}$$

$$SV_{corr} = \begin{bmatrix} \phi_{corr} \\ \theta_{corr} \\ \psi_{corr} \end{bmatrix}, SV_{ORF} = \begin{bmatrix} \phi_{orb} \\ \theta_{orb} \\ \psi_{orb} \end{bmatrix}, SV_{att} = \begin{bmatrix} \phi_{att} \\ \theta_{att} \\ \psi_{att} \end{bmatrix} \tag{15.4}$$

3.1.2.3 R_{IIRF} computation

In view of Fig. 3 and Eq. (14.4), we get:

$$\vec{T} = \vec{R}_S + \vec{R}_{IIRF} \tag{16.1}$$

$$(R_e + h)\begin{bmatrix} C_{L_T} S_{\Delta\lambda_T} \\ -S_{L_T} \\ C_{L_T} C_{\Delta\lambda_T} \end{bmatrix} = R_S \begin{bmatrix} C_{L_S} S_{\Delta\lambda_S} \\ -S_{L_S} \\ -C_{L_S} C_{\Delta\lambda_S} \end{bmatrix} + R_{IIRF} \begin{bmatrix} \widehat{R}_{GEOS,x} \\ \widehat{R}_{GEOS,y} \\ \widehat{R}_{GEOS,z} \end{bmatrix} \tag{16.2}$$

R_{IIRF} can be obtained from Eq. (16.1) as follows:

$$|\vec{T}| = |\vec{R}_S + \vec{R}_{IIRF}| \tag{17.1}$$

$$(R_e + h)^2 = R_{IIRF}^2 + R_s^2 + 2R_{IIRF}R_sC_{\alpha_s} \tag{17.2}$$

$C_{\alpha s} = -$ dot product of unit vectors $\widehat{R}_s$ and $\widehat{R}_{IIRF}$
$= -\widehat{R}_{GEOS,x}C_{Ls}S_{\Delta\lambda s} + \widehat{R}_{GEOS,y}S_{Ls} + \widehat{R}_{GEOS,z}C_{Ls}C_{\Delta\lambda s}$

Solution of the quadratic Eq. (17.2) leads to:

$$R_{IIRF} = R_S/r \tag{17.3}$$

$$r = \left\{C_{\alpha_s} - \sqrt{c_{\alpha_s}^2 - c_{\alpha_{so}}^2}\right\}^{-1}$$
$$C_{\alpha_{so}}^2 = 1 - [(R_e + h)/R_s]^2 \tag{17.4}$$

Note that the parameter r is the same as A (α) in [1] and r in [11] and was called earth curvature parameter by Kamel because its value is dependent on Earth curvature. R_e is obtained from Eq. (12.3) with S_{LT} from the middle row of Eq. (16.2):

$$s_{L_T} = R_s\left(S_{L_S} - \frac{\widehat{R}_{GEOS,y}}{r}\right)/(R_e + h) \tag{17.5}$$

Note that because S_{LT}^2 is multiplied by small number in Eq. (12.3), one or two iterations using Eqs. (12.3), (17.4) and (17.5), starting with $R_e = R_{eo}$ in Eqs. (17.4) and (17.5), should be sufficient to get accurate values for R_e and r.

Note also that if $C_{\alpha_s}^2 < C_{\alpha_{so}}^2$, $\sqrt{c_{\alpha_s}^2 - c_{\alpha_{so}}^2}$ in Eq. (17.4) is imaginary indicating that the image pixel (E_{LRF}, N_{LRF}) corresponds to a point outside earth and (E_{GEOS}, N_{GEOS}) transition from earth to space will be undefined. This can be avoided if a fictitious earth with $C_{\alpha_{so}} = C_{\alpha_s}$ is used in Eq. (17.4) for the space portion of the earth images. In this case, Eqs. (17.3) and (17.4) lead to:

$$r = \frac{1}{c_{\alpha_s}}, R_{IIRF} = R_SC_{\alpha_s} \tag{17.6}$$

3.1.2.4 GEOS Coordinate Computation

In view of Fig. 3, we get:

$$\vec{R}_{IIRF0} = \vec{R}_{IIRF} + \Delta\vec{R}_s \tag{18.1}$$

$\vec{R}_{IIRF0}$ from Eqs. (14.4) and (17.3) or (17.6),

$$\Delta\vec{R}_s = \vec{R}_s - \vec{R}_{s0} = \begin{bmatrix} R_sC_{L_s}S_{\Delta\lambda_s} \\ -R_sS_{L_s} \\ R_{so} - R_sC_{Ls}C_{\Delta\lambda_s} \end{bmatrix} \tag{18.2}$$

(E_{GEOS}, N_{GEOS}) are obtained from Figs. 2 and 3 and Eqs. (18.1) and (18.2):

$$\begin{bmatrix} C_{N_{GEOS}} S_{E_{GEOS}} \\ -S_{N_{GEOS}} \\ C_{N_{GEOS}} C_{E_{GEOS}} \end{bmatrix} = \begin{bmatrix} \widehat{R}_{GEOS0,x} \\ \widehat{R}_{GEOS0,y} \\ \widehat{R}_{GEOS0,z} \end{bmatrix} = \frac{\vec{R}_{IIRF} + \Delta\widehat{\vec{R}}_{s}}{|\vec{R}_{IIRF} + \Delta\vec{R}_{s}|} \tag{18.3}$$

$$E_{GEOS} = \text{Arc tan}\left[\frac{\hat{R}_{GEOS0,x}}{\hat{R}_{GEOS0,z}}\right] \tag{18.4}$$

$$N_{GOES} = -\text{Arc sin}\,\hat{R}_{GEOS0,y} \tag{18.5}$$

$$Z = \left[\frac{E_{GEOS}}{N_{GOES}}\right] \tag{18.6}$$

Note that for star measurements, Z is obtained directly from Eq. (14.4) and Sect. 3.1.2.3 skipped because $\Delta\vec{R}_S$ is insignificant compared to $\vec{R}_{IIRF}$ in Eq. (18.3).

3.2 *KF Initial Conditions*

KF initial conditions are given by:
t_0 = epoch time = UTC_0 at KF start.
$x_0^+ = SV_{KF}$ at epoch = 0_{12+2m}

$$P_0^+ = \text{error covariance matrix at epoch} = \begin{bmatrix} P_{corr,0} & 0_{6\times6} & 0_{6\times2m} \\ 0_{6\times6} & P_{orb,0} & 0_{6\times2m} \\ 0_{2m\times6} & 0_{2m\times6} & P_{ma,0} \end{bmatrix} \tag{19.1}$$

$$P_{corr,0} = \sigma^2_{corr,0}\begin{bmatrix} I_{3\times3} & 0_{3\times3} \\ 0_{3\times3} & 0_{3\times3} \end{bmatrix},\ P_{orb,0} = \sigma^2_{orb,0}\begin{bmatrix} I_{3\times3} & 0_{3\times3} \\ 0_{3\times3} & 0_{3\times3} \end{bmatrix}$$
$$P_{ma,0} = \sigma^2_{ma,0}\begin{bmatrix} I_{m\times m} & 0_{m\times m} \\ 0_{m\times m} & 0_{m\times m} \end{bmatrix} \tag{19.2}$$

$\sigma_{corr,0} \cong \sigma_{orb,0} \cong \sigma_{ma,0} \cong 5.0E-05$ for simulation.

3.3 *KF Detailed Computation*

After level 1 A data block searched for landmarks and determined landmarks are time tagged, KF propagates (t_0, x_0^+, P_0^+) from last event prior to this data block and re-initialized after the(t_1, x_1^+, P_1^+) estimation as shown in Fig. 1. If no landmarks found within the data block, go to end of block of Eq. (21). Otherwise, let LM_T = total number of determined landmarks within the data block and do the following:

For $k = 1$ to LM_T do to **ENDFOR**

$$\Delta t = t_1 - t_0, t_1 = UTC_k \text{ time at landmark number k.} \tag{20}$$

Propagation: From step number 1 of Sect. 3.
Estimation: From step number 2 of Sect. 3.
Re-initialize KF: From step number 3 of Sect. 3.
ENDFOR

At end of data block, do the following:

$$\Delta t = t_1 - t_0, t_1 = UTC_{end} = \text{time at end of data block} \tag{21}$$

Propagation: From step number 1 of Sect. 3.
Re-initialize KF: $(t_0, x_0^+, P_0^+) = (t_1, x_1^+, P_1^+) = (t_1, x_1^-, P_1^-)$
Compute SV_{INR} from x_1^+ using Sect. 2. This is needed for Sect. 6.

If maneuver delta V provided by FDS

At maneuver, do the following:

$$\Delta t = t_1 - t_0, t_1 = UTC_{maneuver} = \text{ maneuver time} \tag{22.1}$$

Propagation: From step number 1 of Sect. 3.
Re-initialize KF:

$$x_1^+ = x_1^- + \Delta x \tag{22.2}$$

$$P_1^+ = P_1^- + \Delta P \tag{22.3}$$

$$\Delta x = \left[0_{1\times 9} \frac{\Delta v_{FDS,r}}{R_{so}} \frac{\Delta v_{FDS,\lambda}}{R_{so}} \frac{\Delta v_{FDS,L}}{R_{so}} 0_{1\times 2m} \right]^T \tag{22.4}$$

$$\Delta P = \text{ diagonal terms 10 to 12 from delta v error analysis.}$$

$$(t_0, x_0^+, P_0^+) = (t_1, x_1^+, P_1^+) \tag{22.5}$$

Compute SV_{INR} from x_1^+ using Sect. 2. This is needed for Sect. 6.

If orbit is delta V provided by FDS instead of delta V

At maneuver, do the following:

$$\Delta t = t_1 - t_0, t_1 = UTC_{OD} = \text{orbitdeterminationtime} \tag{23.1}$$

Propagation: From step number 1 of Sect. 3.
Re-initialize KF:

$$x_1^+ = x_1^- + \delta x \tag{23.2}$$
$$P_1^+ = P_1^- + \delta P \tag{23.3}$$
$$\delta x = \begin{bmatrix} 0_{1\times 6} & \delta\left(\dfrac{\Delta R_s}{R_{so}}\right) & \delta\,\Delta\lambda_s & \delta\,L_s & 0_{1\times(3+2m)} \end{bmatrix}^T \tag{23.4}$$

$$\begin{aligned}(\delta\,\Delta R_s, \delta\,\Delta\lambda_s) = {} & (R_{FDS}, \Delta\lambda_{FDS}, L_{FDS})^- \text{ before OD} \\ & - (R_{FDS}, \Delta\lambda_{FDS}, L_{FDS})^+ \text{ after OD}\end{aligned} \tag{23.5}$$

$$\delta P = \text{diagonal terms 7 to 9 from OD error analysis.}$$
$$(t_0, x_0^+, P_)^+ = (t_1, x_1^+, P_1^+) \tag{23.6}$$

Compute SV_{INR} from x_1^+ using Sect. 2. This is needed for Sect. 6.

Transition matrix A: From Sect. 2.3.

Process noise covariance matrix Q: From Ref. [13], Eqs. (13)–(83) and (13)–(89), we get:

$$Q(\Delta t) = V_0 + V\Delta t + \frac{1}{2}[F_x V + V F_x^T]\Delta t^2 + \frac{1}{3}F_x V F_x^T \Delta t^3 \tag{24.1}$$

$$V_0 = \begin{bmatrix} V_{corr,0} & 0_{6\times 6} & 0_{6\times 2m} \\ 0_{6\times 6} & V_{orb,0} & 0_{6\times 2m} \\ 0_{2m\times 6} & 0_{2m\times 6} & V_{ma,0} \end{bmatrix}, \quad V_{y,0} = \begin{bmatrix} \sigma_{e,y}^2 I_{3\times 3} & 0_{3\times 3} \\ 0_{3\times 3} & 0_{3\times 3} \end{bmatrix} \tag{24.2}$$

$$V = \begin{bmatrix} V_{corr} & 0_{6\times 6} & 0_{6\times 2m} \\ 0_{6\times 6} & V_{orb} & 0_{6\times 2m} \\ 0_{2m\times 6} & 0_{2m\times 6} & V_{ma} \end{bmatrix}, \quad V_y = \begin{bmatrix} \sigma_{\nu,y}^2\, I_{3\times 3} & 0_{3\times 3} \\ 0_{3\times 3} & \sigma_{u,y}^2\, I_{3\times 3} \end{bmatrix} \tag{24.3}$$

where,

y = corr, orb, or ma. For ma, 3 replaced by m.
σ_e = measurement white noise standard deviation, rad.
σ_ν = random walk standard deviation, rad/sec$^{1/2}$.
σ_u = rate random walk standard deviation, rad/sec$^{3/2}$.

$$F_X = \begin{bmatrix} F_{corr} & 0_{6\times 6} & 0_{6\times 2m} \\ 0_{6\times 6} & F_{orb} & 0_{6\times 2m} \\ 0_{2m\times 6} & 0_{2m\times 6} & F_{ma} \end{bmatrix}, \quad F_{corr} = \begin{bmatrix} 0_{3\times 3} & I_{3\times 3} \\ 0_{3\times 3} & 0_{3\times 3} \end{bmatrix} \tag{25.1}$$

F_{orb} from Euler-Hill equations:

$$F_{orb} = \begin{bmatrix} 0_{3\times 3} & I_{3\times 3} \\ \omega_e^2\, F_{21} & 2\,\omega_e\, F_{22} \end{bmatrix} \cong \begin{bmatrix} 0_{3\times 3} & I_{3\times 3} \\ 0_{3\times 3} & 0_{3\times 3} \end{bmatrix} \tag{25.2}$$

$$F_{21} = \begin{bmatrix} 3 & 0 & 0 \\ 0 & 0 & 0 \\ 0 & 0 & -1 \end{bmatrix}, F_{22} = \begin{bmatrix} 0 & 1 & 0 \\ -1 & 0 & 0 \\ 0 & 0 & 0 \end{bmatrix}, F_{ma} = \begin{bmatrix} 0_{mxm} & I_{mxm} \\ 0_{mxm} & 0_{mxm} \end{bmatrix} \tag{25.3}$$

This leads to:

$$Q(\Delta t) = \begin{bmatrix} Q_{corr} & 0_{6\times 6} & 0_{6\times 2m} \\ 0_{6\times 6} & Q_{orb} & 0_{6\times 2m} \\ 0_{2m\times 6} & 0_{2m\times 6} & Q_{ma} \end{bmatrix} \tag{25.4}$$

$$Q_y = \begin{bmatrix} \left(\sigma_{e,y}^2 + \sigma_{v,y}^2\,\Delta t + \frac{1}{3}\,\sigma_{u,y}^2\,\Delta t^3\right) I_{3\times 3} & \frac{1}{2}\,\sigma_{u,y}^2\,\Delta t^2 I_{3\times 3} \\ \frac{1}{2}\,\sigma_{u,y}^2\,\Delta t^2 I_{3\times 3} & \sigma_{u,y}^2\,\Delta t I_{3\times 3} \end{bmatrix} \tag{25.5}$$

where,

y = corr, orb, or ma. For ma, $I_{3\times 3}$ is replaced by I_{mxm}.

Note that the first element of the above matrix is the same as in [13], Eq. (7)–(143).

The sigma values can be computed using Eq. (25.5), SV_{INR} error analysis and estimate of time between measurements. For simulation, this leads to:

$(\sigma_{e,corr,}\ \sigma_{e,orb,}\ \sigma_{e,ma}) = (1.942E-07, 0, 0)$ rad.

$(\sigma_{\nu,corr}, \sigma_{\nu,orb}, \sigma_{\nu,ma}) = (4.8E-07, 0, 1.269E-09)$ rad/s$^{1/2}$.

$(\sigma_{u,corr}, \sigma_{u,orb}, \sigma_{u,ma}) = (4.774E-10, 9.32E-13, 2.318E-11)$ rad/s$^{3/2}$.

Landmark measurement noise covariance matrix R:

$R = \sigma_M^2 I_{2\times 2}$

σ_M = sigma measurement noise calculated from landmark determination error analysis (=0.1 pixel for simulation).

Landmark location sensitivity matrix H:

H is determined from $(\frac{\partial Z}{\partial x})_{x=0}$ where Z is the estimated landmark measurement from Sect. 3.1.2 using the linear representation of C_{IIRF}^{GEOS} of Eq. (15.1). After some laborious algebraic manipulation, we get:

$H = 2 \times (12 + 2m)$ matrix given by:

$$H = \left(\frac{\partial Z}{\partial x}\right)_{x=0} = [H_{corr} \quad H_{orb} \quad H_{ma}] \tag{26.1}$$

where,

$$H_{corr} = -\begin{bmatrix} T_{\bar{N}} S_{\bar{E}} & 1 & T_{\bar{N}} C_{\bar{E}} & 0_{1\times 3} \\ C_{\bar{E}} & 0 & -S_{\bar{E}} & 0_{1\times 3} \end{bmatrix} \tag{26.2}$$

For Spacecraft x axis parallel to earth equator (e.g., COMS):

$$H_{orb} = -\begin{bmatrix} 0 & 1 & T_{\bar{N}} S_{\bar{E}} & 0_{1\times 3} \\ 0 & 0 & C_{\bar{E}} & 0_{1\times 3} \end{bmatrix} + \bar{r} \begin{bmatrix} \frac{S_{\bar{E}}}{C_{\bar{N}}} & \frac{C_{\bar{E}}}{C_{\bar{N}}} & 0 & 0_{1\times 3} \\ C_{\bar{E}} S_{\bar{E}} & -S_{\bar{E}} S_{\bar{N}} & C_{\bar{N}} & 0_{1\times 3} \end{bmatrix} \tag{26.3}$$

For Spacecraft x axis parallel to orbit plane (e.g., GOES I-M):

Replace $\begin{bmatrix} 0 & 1 & T_{\bar{N}}S_{\bar{E}} & 0_{1\times3} \\ 0 & 0 & C_{\bar{E}} & 0_{1\times3} \end{bmatrix}$ by $\begin{bmatrix} 0 & 1 & T_{\bar{N}}S_{\bar{E}} & 0_{1\times2} & T_{\bar{N}}C_{\bar{E}}/\omega_e \\ 0 & 0 & C_{\bar{E}} & 0_{1\times2} & -S_{\bar{E}}/\omega_e \end{bmatrix}$

$$\bar{r} = \left(C_{\bar{\alpha}_s} - \sqrt{C_{\bar{\alpha}_s}^2 - 1 + ((R_e + h)/R_{so})^2}\right)^{-1} \tag{26.4}$$

$$C_{\bar{\alpha}_s} = \mathrm{Cos}\bar{\alpha}_s = C_{\overline{N}} = C_{\overline{E}} \tag{26.5}$$

$T_{\overline{N}} = \mathrm{Tan}\overline{N}_{GEOS},\ S_{\overline{N}} = \mathrm{Sin}\overline{N}_{GEOS},\ C_{\overline{N}} = \mathrm{Cos}\overline{N}_{GEOS}$

$S_{\overline{E}} = \mathrm{Sin}\overline{E}_{GEOS}\ ,\ C_{\overline{E}} = \mathrm{Cos}\overline{E}_{GEOS}$

$(\overline{E}_{GEOS}\ ,\ \overline{N}_{GEOS})$ = landmark location from Eq. (13.4).

R_e = earth radius at landmark location from Eq. (12.3).

h = landmark altitude.

For star measurements, $r = 0$ and H_{orb} becomes insensitive to orbit translational part ($\delta R/R_{so}$, $\delta\lambda$, δL). Therefore, stars cannot be used to refine orbit and, therefore, orbit refinement must be deleted from KF as described in Sect. 5.1.

$$H_{ma} = \begin{bmatrix} C_{11} & C_{12} & 0 & 0 \\ C_{21} & C_{22} & 0 & 0 \end{bmatrix} \tag{26.6}$$

$$C_{11} = -\frac{C_{22}}{C_{\overline{N}}}\ ,\ C_{12} = -\frac{C_{21}}{C_{\overline{N}}}\ ,\ C_{21} = -\frac{S_{\overline{E}} - C_{\overline{N}}}{1 - C_{\overline{N}}S_{\overline{E}}}\ ,\ C_{22} = -\frac{S_{\overline{N}}C_{\overline{N}}}{1 - C_{\overline{N}}S_{\overline{E}}} \tag{26.7}$$

H_{ma} for two mirror imaging systems to be investigated in the future.

3.4 Thermo-Elastic Model Time Series

The thermo-elastic $SV_{ma,model}$ and $SV_{corr,model}$ time series can be obtained form Eqs. (2.1)–(3.2) as follows:

1. Create daily time series at, e.g., one-minute interval for, e.g., seven days using interpolation of SV_{ma} and SV_{corr} data at time $t_{i,n}$, $i = 1, 2, \ldots, 1440$ and $n = 1, 2 \ldots, 7$.
2. The $SV_{ma,model}(t_{i,n})$ and $SV_{corr,model}(t_{i,n})$ for the next day ($n = 8$) are obtained by averaging the last seven days of $SV_{ma}(t_{i,n})$ and $SV_{corr}(t_{i,n})$ data:

$$SV_{ma,model}(t_{i,8}) = \frac{1}{7}\sum_{n=1}^{n=7} SV_{ma}(t_{i,n}) \tag{27.1}$$

$$SV_{corr,model}(t_{i,8}) = \frac{1}{7}\sum_{n=1}^{n=7} SV_{corr}(t_{i,n}) \tag{27.2}$$

Note that $SV_{ma,model}$ and $SV_{corr,model}$ are initially determined by analysis or set to zero.

3. Repeat above process once a day using one-day sliding window.

4 Simulation Results

A hundred landmarks distributed over earth and COMS imaging schedule were used in the simulation [14, 15]. The true $\overline{SV}_{INR}$ is calculated using eccentricity =0.0001, inclination = 0.05°, $SV_{ma,model}$ and $SV_{corr,model}$ amplitudes = 100 µrad, with 24-h period, and attitude amplitude = 300 µrad with 2.4-h period. The maneuver delta V times are obtained from [16], Fig. 8, and magnitudes from [17], Tables 2.

The estimated SV_{INR} are shown in Fig. 4 for seven days and is computed using Sect. 3.3 based on $SV_{ma,model}$ and $SV_{corr,model}$ errors =10 µrad, FDS maneuver delta V errors from [17], Table 3 (or FDS orbit determination error from Table 7). Figure 5 shows SV_{errors}, $\delta\, SV = \overline{SV}_{INR} - SV_{INR}$. Figure 6 shows residual errors computed using Sect. 3.1. The simulated landmarks are obtained using the true $\overline{SV}_{INR}$ to transfer $(\bar{E}_{GEOS}, \bar{N}_{GEOS})$ to $(\bar{E}_{LRF}, \bar{N}_{LRF})$ based on Sect. 3.1.2 inverse transformation. The estimated (E_{LRF}, N_{LRF}) are then obtained from actual $(\bar{E}_{LRF}, \bar{N}_{LRF})$ by adding a random normal distribution land- mark determination error with $\sigma_M = 2.8E\text{-}06\,\text{rad}$ for visible landmarks and $\sigma_M = 11.2E\text{-}06\,\text{rad}$ for IR landmarks. Simulation was also successfully used to stress test the basic method for cases using eccentricity = 0.001, inclination = 0.5°, $SV_{ma,model}$ and $SV_{corr,model}$ amplitudes = 1000 µrad with errors =100 µrad and only IR landmarks.

5 Adaptation to Other Systems

The following 3 subsections show how the basic method described in Fig. 1 can be adapted to be used for systems based on star and landmark measurements, star only measurements with orbit from FDS or GPS, and systems with attitude rate telemetry inserted in the image wideband data.

5.1 Systems Based on Star and Landmark Measurements

For stars:

- KF refinements $(\delta\, R_s/R_{so}, \delta\, \lambda_s, \delta\, L_s) = (0,0,0)$ and $(x_{orb}, \dot{x}_{orb})$ deleted from KF state vector.
- Rows and columns associated with $P_{orb,0}$, A_{orb}, P_{orb} and F_{orb} deleted from P_0^+, A, V, V_0, and F_x.
- H_{orb} deleted from H.
  In this case:

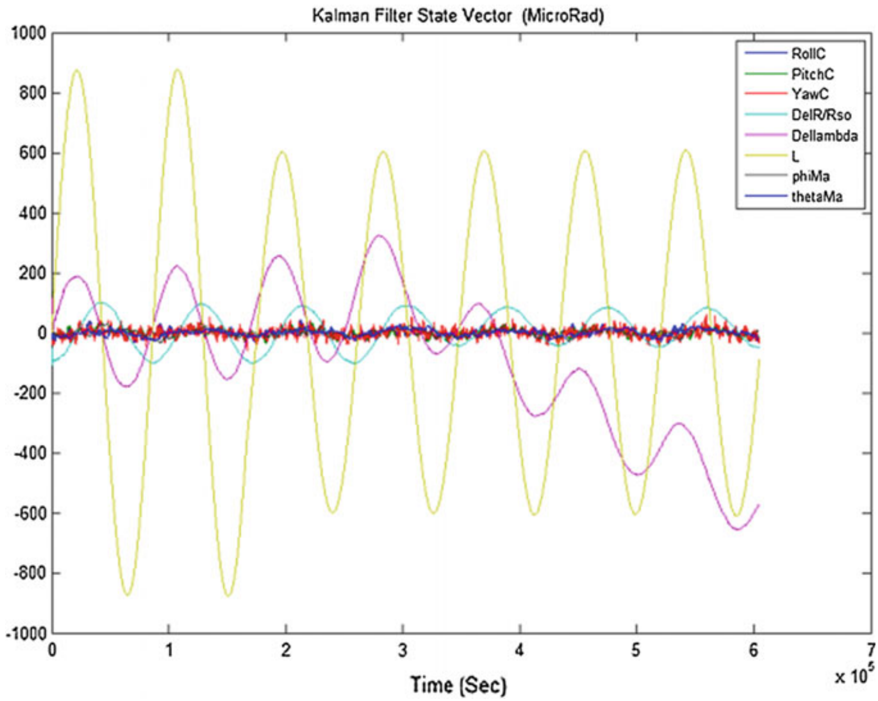

Fig. 4 KF state vector

- one star per minute or 3 stars per 5 min are sufficient to determine KF x_{corr} and x_{ma}.
- SV_{KF} dimension $= 6 + 2m$ instead of $12 + 2m$.
- KF detailed computation is like basic method with landmarks replaced by stars. For landmarks:
- Use KF for orbit refinements ($\delta\, R_s/R_{so}$, $\delta\, \lambda_s$, $\delta\, L_s$) using the above deleted items. In this case:
- Few landmarks (e.g.,10 well distributed landmarks over earth) are sufficient to determine (x_{orb}, $\dot{x}_{orb}$).
- SVKF dimension $= 6$ instead of $12 + 2m$.

5.2 *Systems Based on Star only Measurements*

- KF is same as in Sect. 5.1 for stars. In this case, the orbit must be provided by FDS or GPS.

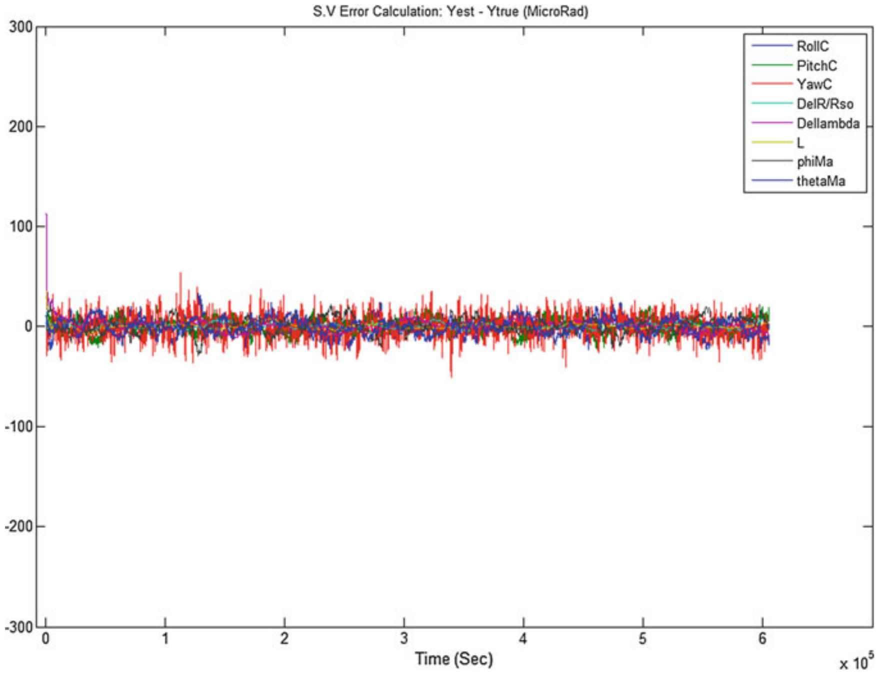

Fig. 5 SV errors $\delta\,SV = SV_{INR} - SV_{INR}$

5.3 Systems Based on Inertial Angular Rate Telemetry

The $(\omega_{sx}, \omega_{sy}, \omega_{sz})$ telemetry represent inertial angular rate along ACF axes in the form of time series spaced at Δt_{att} (e.g., 0.01 s) inserted in the imager wideband data. The rates SV_{ACF} of Eq. (15.3) can be obtained from $(\omega_{sx}, \omega_{sy}, \omega_{sz})$ using Fig. 3 with IIRF replaced by ACF. Starting with $\dot{\theta} + \omega_e$ about $-Y_{GEOS}$ axis followed by $\dot{\phi}$ about the new $-X$ axis followed by $\dot{\psi}$ about $-Z_{ACF}$ axis and using Eqs. (14.5) and (15.1), we get:

$$\begin{bmatrix} \omega_{sx} \\ \omega_{sy} \\ \omega_{sz} \end{bmatrix} = -\dot{\psi} \begin{bmatrix} 0 \\ 0 \\ 1 \end{bmatrix} - \dot{\phi} \begin{bmatrix} C_\psi \\ S_\psi \\ 0 \end{bmatrix} - (\dot{\theta} + \omega_e) \begin{bmatrix} S_\psi C_\phi \\ C_\psi C_\phi \\ S_\phi \end{bmatrix} \tag{28.1}$$

This leads to:

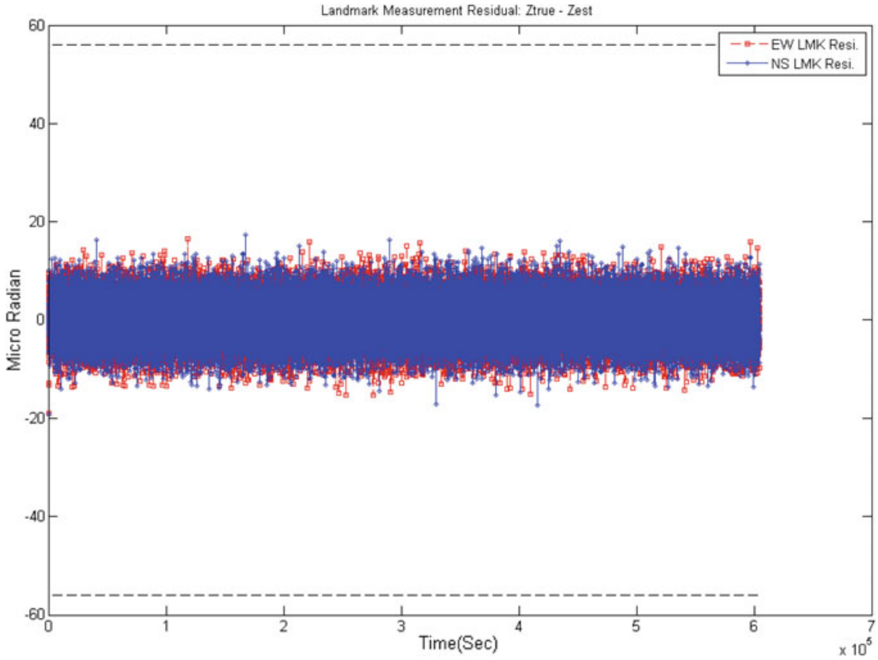

Fig. 6 Landmarks measurement residuals

$$
\begin{aligned}
S\dot{V}_{ACF} = \begin{bmatrix} \dot{\phi} \\ \dot{\theta} \\ \dot{\phi} \end{bmatrix} &= -\begin{bmatrix} \omega_{sy} S\,\psi + \omega_{sx} C\,\psi \\ \omega_e + (\omega_{sy} C\,\psi - \omega_{sx} S\,\psi)/C\,\phi \\ \omega_{sx} - (\omega_{sy} C\,\psi - \omega_{sx} S\,\psi) S\,\phi\,/C\,\phi \end{bmatrix} \\
&\cong -\begin{bmatrix} \omega_{sx} + \omega_{sy}\,\psi \\ \omega_{sy} + \omega_e - \omega_{sx}\,\psi \\ \omega_{sz} - \omega_{sy}\,\phi \end{bmatrix}
\end{aligned} \tag{28.2}
$$

Note that Eq. (28.2) can also be obtained from [13], Appendix E Table E-2 for 2, 1, 3 type rotation by replacing (ϕ, ψ) with $-(\phi, \psi)$ and $(\omega_I, \omega_J, \omega_K)$ with $(\omega_{sy}, \omega_{sx}, \omega_{sz})$ on the right side of the equation and replacing $(\dot{\phi}, \dot{\theta}, \dot{\psi})$ with $-(\dot{\theta} + \omega_e, \dot{\phi}, \dot{\psi})$ on the left side of the equation.

Now, the SV_C time series spaced by Δt_{att} over $\Delta t = t_1 - t_0$ is computed as follows: Let $j = \text{Integer}(\Delta t/\Delta tatt)$

For $i = 1, \ldots, j$ plus final step from τ_j to t_1

$$SV_{ACF}(\tau_i) = SV_{ACF}(\tau_{i-1}) + S\dot{V}_{ACF}(\tau_{i-1})\Delta t_{att} \tag{28.3}$$

where

$$S\dot{V}_C(\tau_{i-1}) = S\dot{V}_{ACF}(\tau_{i-1}) + S\dot{V}_{corr,model}(\tau_{i-1}) + \dot{x}corr(\tau_{i-1}) \tag{28.4}$$

With

$$SV_C(\tau_i) = SV_{ACF}(\tau_i) + SV_{Corr,model}(\tau_i) + x_{corr}(\tau_i) \tag{28.5}$$

$SV_{corr,model}$ obtained from Sect. 3.4 and x_{corr} determined by KF and defined in Eqs. (8.2) and (8.3).

At KF start (see Sects. 3.2 and 3.4):

$$SV_{KF} = 0_{12+2m} \text{ and } SV_{corr,model} = 0_3 \tag{29.1}$$

In view of Eqs. (15.2), (15.3), and (6.1) to (6.3)

$$SV_C(0) = SV_{ACF}(0) = SV_{ORF}(0) + SV_{att}(0) \tag{29.2}$$

$$SV_{att}(0) \text{ from telemetry or } = 0_3. \tag{29.3}$$

At KF re-initialization (see Fig. 1):

$$SV_C(0) = SV_C(t_1) \text{ from Eq. (28.4)} \tag{29.4}$$

$$SV_{ACF}(0) = SV_{ACF}(t_1) \text{ from Eq. (28.3)} \tag{29.5}$$

$$\dot{SV}_{ACF}(0) = \dot{SV}_{ACF}(t_1) \text{ from Eq. (28.2)} \tag{29.6}$$

Note that SV_{ACF} of Eq. (28.4) is corrected by x_{Corr} determined by KF to compensate for gyro drift and the first part of H_{orb} in Eq. (26.3) must be deleted.

6 Image Registration Using Resampling

Image registration requires two steps. The first step is to transfer level 1A (column, line) pixel indices (c, ℓ) to $(c', \ell') = (c, \ell) + (\Delta c, \Delta\ell)_{,\ell}$ in the GEOS fixed frame. The second step is to resample (c', ℓ') pixels to generate level 1B data block (see, e.g., [18]). The first step can be performed using Sect. 3.1.2 algorithm to determine $(\Delta\ell, \Delta\ell)_{c,\ell}$ from $(\Delta E, \Delta N)_{c,\ell} = (E_{GEOS}, N_{GEOS})_{c,\ell} - (E_{LRF}, N_{LRF})_{c,\ell}$ divided by pixel size. Index c and N_{LRF} are fixed over pixel line and index c and E_{LRF} are fixed over pixel column. The SV_{INR} time series needed for (c, ℓ) to (c', ℓ') transformation is obtained from Sect. 2.3. The processing time of this transformation is significantly reduced by computing $(\Delta C, \Delta L)_C, L$ for a subset of pixels (C, L) uniformly distributed over the level 1A (c, ℓ) array. The $(\Delta C, \Delta L)_C, L$ for the remaining pixels are then computed by EW and NS linear interpolation between the $(\Delta C, \Delta L)_{C,L}$ subset. Note that the number of (C, L) pixel subset is obtained by analysis of SV_{INR} and attitude jitter effects on registration error. Note also that level 1 A block should be slightly larger than level 1B block to account for the shift caused by orbit, attitude, and misalignment variation over time.

7 Conclusion

INR and KF state vectors suitable for the new INR method were defined. The basic method is based on landmark measurements to determine orbit, attitude correction angles, and imager misalignments with maneuvers delta V (or orbit with coarse accuracy) provided by FDS. The method was proven by simulation. Adaptation of this method to other INR systems and an algorithm for transferring pixels from LOS to the fixed grid GEOS frame needed for pixel data resampling are presented.

Acknowledgements The authors appreciate the support of Eun-joo Kwon and J.B. Park during the simulation effort.

References

1. Kamel AA (1996) GOES image navigation and registration system. SPIE 2812:766–776
2. Lu F et al (2008) Image Navigation for the FY2 geosynchronous meteorological satellite. J Atmos Ocean Tech 25:1149–1165. Accessed 1 July 2008
3. Woo J et al (2011) Analysis of COMS MI image navigation and registration performance, ISRS. Accessed 2–4 Nov 2011
4. Chambon T et al (2013) On-ground evaluation of MTG image navigation and registration (INR) performances. In: Proceedings of SPIE 8889, sensors, systems, and next- generation satellites, vol XVII, p 88891J. Accessed 16 Oct 2013
5. Okuyama A et al (2015) Preliminary validation of Himawari-8/AHI navigation and calibration. Accessed 9 Nov 2015
6. Kamel AA (1999) Precise spacecraft camera image navigation and registration, US patent #5,963,166, 5 Oct 1999
7. Carr JL (2009) Twenty-five years of INR. J Astronaut Sci 57:505–515
8. Harris J et al (2009) Image navigation and registration improvements using GPS. In: Geoscience and remote sensing symposium, 2009 IEEE international. IGARSS, vol 3, pp 247–250
9. De Luccia FJ et al (2016) Image navigation and registration performance assessment tool set for the GOES-R advanced baseline imager and geostationary lightning mapper. Accessed 4 April 2016
10. GOES Earth Location User's Guide (ELUG), DRL 504-11 Revision 1, Appendix C, NOAA, March 1998
11. Virgilio VN (2015) Geolocation of remotely sensed pixels by introspective landmarking, US 8942421, 27 Jan 2015
12. Sidi MJ (1997) Spacecraft dynamics and control. Cambridge University Press, Cambridge
13. Wertz JR (1978) Spacecraft attitude determination and control. D. Reidel Publishing, Hingham (1978) (reprinted in 2000 by Kluwer Academic Publisher. Mass, Boston)
14. Final technical report: as part of the deliverables of the contract for technical COMS technical monitoring and services, Contract No. KARI-13-0007. Accessed 18 April 2014
15. Final technical report: as part of the deliverables of the contract for technical COMS technical monitoring and services, Contract No. KARI-15-0012. Accessed 24 April 2015
16. Lee BS et al (2010) East-west station-keeping maneuver strategy for COMS satellite using iterative process. Advances in space research, the official journal of the committee on space research (COSPAR)
17. Hwang Y et al (2008) Orbit determination accuracy improvement for geostationary single station antenna tracking. ETRI J 30(6):774–782
18. Ormiston JP et al (2008) GOES advanced baseline imager – ground processing development system, 5th GOES users' conference. Accessed 23 Jan 2008